Dielectric Loaded and Covered Rectangular Waveguide Phased Arrays

By V. GALINDO AND C. P. WU

(Manuscript received September 11, 1967)

This study examines the effects of loading or covering a phased array with dielectric materials. It studies in detail the effect of dielectric geometry, dielectric constant, and sheath thickness on the wide angle array performance of an array of rectangular waveguides in the H and quasi-E plane modes of scan. We obtain numerical solutions of the integral equations describing an array covered with thick dielectric material. The results show that we can obtain a match over a wide scan angle for the array by appropriate use of dielectric geometries, and we discuss the advantages and disadvantages of several geometries.

I. INTRODUCTION

The advent of swift aircraft, missile warfare, and the need for modern radar to accomplish multifunction detection has given impetus for a considerable amount of research into phased-array antennas. Such arrays consist of a large group of small radiators in a grid, frequently a rectangular grid, and, most important, correlated in phase and amplitude. The radiated beam can be steered by an electronically-variable linear taper of the phase correlation among elements. (See Fig. 1).

Considerable knowledge of the behavior and problems of such arrays has been obtained in recent years by experimental and theoretical study of phased linear and parallel plate arrays. For example, it is well known that the coupling coefficients between any single excited element in the array and any terminated inactive element is uniquely determined by the inverse Fourier series transform of the reflection coefficient as a function of scan angle determined when all elements are excited.[1] Hence, by studying the array behavior for all possible linear tapers of phase, we can determine the behavior of the array for any phase or amplitude distribution among the elements.

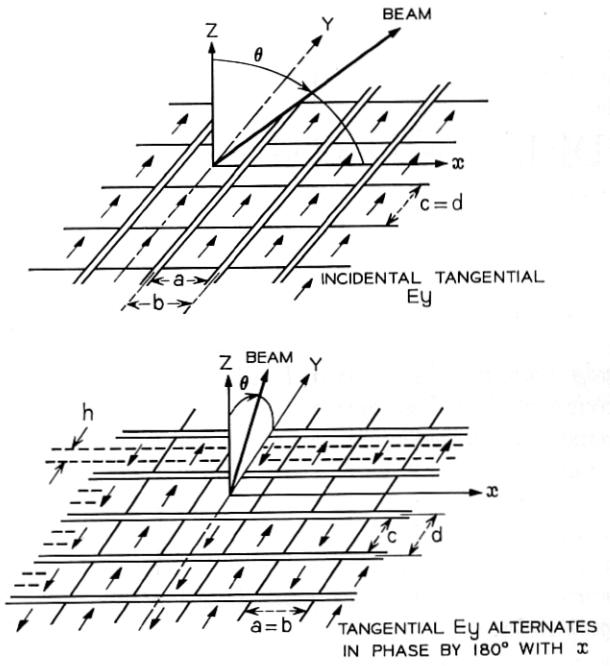

Fig. 1 — Infinite array geometry. *Top*: H-plane scanning in X-Z plane, *Bottom*: Quasi-E plane scanning in Y-Z plane.

Of fundamental importance in designing such arrays is a knowledge, and control, of the mutual coupling (the coupling coefficients) between elements in an array. For arrays which scan over wide angles, this coupling very seriously affects the array, so substantial effort has been made to understand mutual coupling. Because the arrays of interest are very large and consist of very many elements, theoretical studies have generally assumed the arrays to be infinite in extent. The usefullness of this approximation for elements located near the center of a large array has been verified, and in fact, the approximation is frequently valid to within several elements from the edge.[1]

Because the arrays are generally very large, the coupling between greatly separated elements, the asymptotic coupling, is also of interest and has been theoretically studied.[2, 3] In general, planar phased arrays with terminated elements behave like lossy surfaces and have an asymptotic $1/r^2$ decay of coupling between elements separated by the distance r along the array surface.

Among other fundamental and interesting early developments is that the transmission coefficient of a phased array with all elements excited, as a function of scan angle, is directly related and proportional to the radiation pattern of a single-excited element in the array as a function of far-field observation angle.[4] As we mentioned, the two physical situations (all the elements excited with a linear phase taper and only one element excited) are uniquely related. Hence, an analytical formulation for only one or the other situation is necessary. Although most work has concentrated on the linear phase taper case, with the consequent application of periodicity conditions and Floquet's theorem,[1, 5, 6] some work has proceeded by directly attacking the case with only a single element excited.[7]

One of the most advantageous approaches to phased array problems has been through the use of high-speed computers and numerical solutions of the appropriate integral equations.[5] We use this approach in this study, which attempts to discover some problems and solutions associated with covering phased arrays with radomes. The principal problem is, of course, to maintain a good impedance match to the array over a wide scan angle when the phased array radome is included in the design. Now many antennas have radomes covering their moving mechanical parts and their interior electrical components. A planar phased array can be so protected by covering the array with a dielectric sheath or by loading it with a dielectric material. Hence our study concentrates on this type of cover.

Whereas ordinary radomes usually are designed to have the least effect on the antennas they cover, phased array covers often can be made to very substantially improve the wide angle scan performance of the array. In fact, Magill and Wheeler recently have shown that a dielectric sheath cover can greatly improve the wide angle match of the array.[8] However, their analysis was a transmission line analysis in the sense that it did not take into account the interaction of the evanescent modes, generated at the array interface, with the dielectric sheath.

More recently, Lee[9] has made an analysis restricted to an array of thin-walled parallel plates, wherein the interaction of a limited number of evanescent modes with the dielectric sheath is taken into account. His results bear out the possibility of improving the array match with a dielectric sheath.

By using a somewhat different and more powerful analytical approach, wherein the integral equations describing the array with a

dielectric covering are solved by an accurate numerical technique (basically Galerkin's method[10]), we may obtain a solution with few restrictions. The interaction of virtually all the modes at the array interface with one or more dielectric sheaths is accounted for with very little more difficulty than that entailed in the solution for the uncovered array. We made an extensive study of the rectangular array shown in Fig. 1 by this method for two modes of scan, the quasi-E and H planes of scan.[5] We use the term "quasi-E" because the adjacent columns of elements in the bottom part of Fig. 1 are out of phase by 180°.* We assume that the waveguides in each case are excited in the dominant mode and we compute the parameter of particular interest, the reflection coefficient R of this mode, from the aperture field determined by the integral equations.

We divided the complete study into two parts. The first, considered in this paper, analyzes the effects of loading the waveguide with dielectric or covering the array with a very thick sheath where only one grating lobe, at most, is present in the sheath. Generally speaking, a thick sheath is used with only lower dielectric constant materials because with higher dielectric constants in a thick sheath a great and very frequency-sensitive mismatch arises. Furthermore, the presence of two grating lobes in the sheath gives rise to surface wave phenomenon. This is the subject of the second part of our study, which we have relegated to another part.[11] In that paper we plan to deal with thinner sheaths, multiple sheaths, and some anomolous surface wave effects that we have observed in arrays with dielectric covers.

II. METHOD OF ANALYSIS

Fig. 2 shows the three dielectric geometries that we analyzed. In each case we assume a moderate fixed waveguide wall thickness[5] to exist in the plane of scan only. The top figure illustrates the "loaded" array with a symmetrical iris in the aperture (quasi-E scan only, Fig. 1). Fig. 2 also shows two other thick sheath covers. By "thick" we mean that there is very little interaction between the evanescent modes generated at the aperture plane ($z = 0$) and the second dielectric boundary removed from the array interface ($z = \pm d_s$). We may test the validity of this assumption by estimating the relative amplitudes of the evanescent to propagating modes at $z = \pm d_s$ when the second boundary is not present. We made such a validity check with most

* The waveguides are excited in this manner to reduce to a more easily numerically tractable one-dimensional integral equation the two-dimensional integral equations which result in the usual E-plane scan.

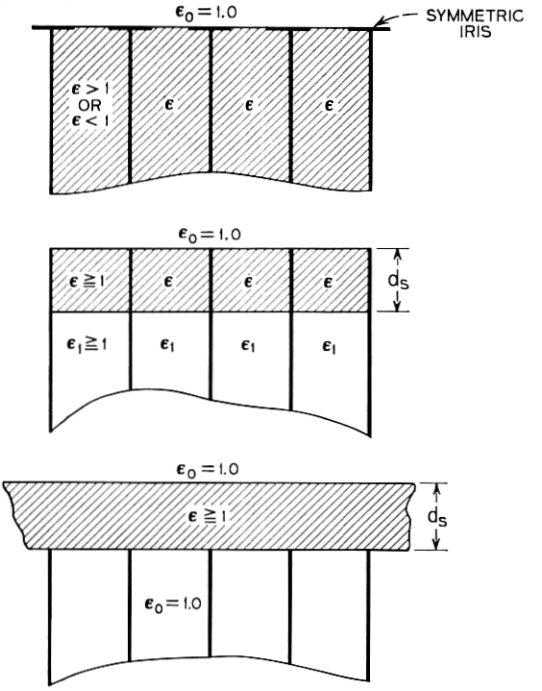

Fig. 2 — Dielectric sheath geometry. *Top*: Dielectric loading. *Middle*: Sheath inside guides. *Bottom*: Sheath outside guides.

of the thick sheath results. Notice that with this assumption the input impedance or reflection coefficient is a periodic function of the distance d_s.

Actually the integral equations that are solved require only a slight modification to go from a "thick" approximation to a "total" accounting of the interaction of higher order modes with the dielectric interface removed from the aperture by d_s. The actual equations solved for the dielectric loaded case take the forms:[5]

$$2Y_0 e_{y_0}(y) = \int_{-h/2}^{h/2} \left[\sum_{0}^{\infty} Y_n e_{y_n}(y) e_{y_n}(y') + \sum_{-\infty}^{\infty} Y'_m \psi_m(y) \psi_m^*(y') \right] E_y(y')\, dy' \tag{1}$$

for the unknown tangential electric field in the aperture in the quasi-E plane scan case, and

$$2Z_1 \varphi_1(x) = \int_{-b/2}^{b/2} \left[\sum_{1}^{\infty} Z_n \varphi_n(x) \varphi_n(x') + \sum_{-\infty}^{\infty} Z'_m \psi_m(x) \psi_m^*(x') \right] H_x(x')\, dx' \tag{2}$$

for the unknown magnetic field over an entire cell ($b \times d$, see Fig. 1). The $\varphi_n(x)$ and $e_{y_n}(y)$ are appropriate interior orthonormal waveguide modes:

$$\begin{cases} \varphi_n = \sqrt{\frac{2}{a}} \begin{matrix} \cos \\ \sin \end{matrix} \left(\frac{n\pi}{a} x\right) \quad \text{for} \quad \left(n = \begin{matrix} \text{odd} \\ \text{even} \end{matrix}\right) \quad \text{in} \quad |x| \leqq \frac{a}{2} \\ \varphi_n = 0 \quad \text{in} \quad \left(\frac{a}{2} < |x| < \frac{b}{2}\right) \end{cases} \tag{3}$$

and

$$\begin{cases} e_{y_n} = -\sqrt{\frac{\epsilon_n}{c}} \begin{matrix} \cos \\ \sin \end{matrix} \left(\frac{n\pi}{c} y\right) \quad \text{for} \quad \left(n = \begin{matrix} \text{even} \\ \text{odd} \end{matrix}\right) \quad \text{in} \quad |y| \leqq \frac{c}{2} \\ e_{y_n} = 0 \quad \text{in} \quad \left(\frac{c}{2} < |y| < \frac{d}{2}\right), \qquad \epsilon_n = \text{Neumann's constant} \end{cases} . \tag{4}$$

The $\psi_m(x)$ or $\psi_m(y)$ are appropriate exterior orthonormal modes pertinent to the periodic structure and are obtained from an application of the Floquet theorem:

$$\begin{cases} \psi_m(x) = \sqrt{\frac{1}{b}} \exp j\left(\frac{2\pi m - kb \sin \theta}{b}\right) x \\ \psi_m(y) = \sqrt{\frac{1}{d}} \exp j\left(\frac{2\pi m - kd \sin \theta}{d}\right) y \end{cases} \qquad k = \frac{2\pi}{\lambda_0}. \tag{5}$$

By the laws of transmission of a plane wave through a plane dielectric boundary (Snell's law), the quantity ($kb \sin \theta$) or ($kd \sin \theta$) is unchanged by the presence of the dielectric. Hence the interior and exterior modes are independent of the dielectric constant. By using the $h \leqq c$ limits in (1) we also allow for the presence of a thin metallic iris directly at the aperture plane (see Fig. 1).

The incident electric field in (1) is given by $e_{y_0}(y) \exp(-j\beta_0^e z)$ and the incident magnetic field in (2) by $\varphi_1(x) \exp(-j\beta_1^h z)$, where the interior modal propagation constants are given by

$$\begin{cases} \beta_n^e = \sqrt{\epsilon k^2 - \left(\frac{\pi}{b}\right)^2 - \left(\frac{n\pi}{c}\right)^2} \quad (\epsilon \text{ appropriate to the region}) \\ \beta_n^h = \sqrt{\epsilon k^2 - \left(\frac{n\pi}{a}\right)^2} \end{cases} , \tag{6}$$

and the exterior propagation constants by

$$\begin{cases} \beta_m'^{e} = \sqrt{\epsilon k^2 - \left(\frac{\pi}{b}\right)^2 - \left(\frac{2\pi m - kd \sin \theta}{d}\right)^2} \\ \beta_m'^{h} = \sqrt{\epsilon k^2 - \left(\frac{2\pi m - kb \sin \theta}{b}\right)^2} \end{cases} . \tag{7}$$

Now the coefficients of the interior and exterior dyads in (1) and (2), the Y_n, Y_m', Z_n, and Z_m', take a form that is dependent on the dielectric sheath geometry. For the dielectric loaded case they become simply the modal admittances and impedances:[5]

$$\begin{aligned} \omega\mu Y_n &= \left[\epsilon k^2 - \left(\frac{\pi}{b}\right)^2\right] \Big/ \beta_n^e , \qquad \omega\mu Y_m' = \left[\epsilon k^2 - \left(\frac{\pi}{b}\right)^2\right] \Big/ \beta_m'^{e} , \\ Z_n &= \omega\mu/\beta_n^h , \qquad Z_m' = \omega\mu/\beta_m'^{h} . \end{aligned} \tag{8}$$

For the dielectric sheath cases, with one or more sheaths, the Y_n, Y_m', Z_n, and Z_m' become the modal admittances or impedances appropriately referred to the aperture plane ($z = 0$). These modal admittances or impedances are obtainable by the usual transmission line equations. For example, suppose a single dielectric sheath inside the guides is considered (middle of Fig. 2) in the quasi-E plane scan case. Define

$$\begin{cases} \gamma_n = \beta_n^e \text{ inside the dielectric in the guide.} \\ \beta_n = \beta_n^e \text{ in the empty portion of the guide.} \\ Y_n = \text{admittance in the dielectric region.} \\ \mathcal{Y}_n = \text{admittance in the air region.} \end{cases} \tag{9}$$

Then the coefficients Y_n become

$$Y_n \to Y_n\left(\frac{\mathcal{Y}_n + jY_n \tan \gamma_n d}{j\mathcal{Y}_n \tan \gamma_n d + Y_n}\right), \tag{10}$$

while the exterior Y_m' coefficients remain unchanged (unless an exterior sheath is simultaneously included). The free term on the left becomes, if we postulate the same incident field as earlier,

$$2Y_0 e_{v_0} \to 2e^{j\beta_0 d}\left(\frac{\mathcal{Y}_0 Y_0 \sec \gamma_0 d}{j\mathcal{Y}_0 \tan \gamma_0 d + Y_0}\right) e_{v_0} . \tag{11}$$

Solving equations (1) and (2) by the Galerkin[10] (or Ritz) method means that (1) and (2) are approximated in an N-dimensional subspace* of the complete Hilbert space.[5] One way of testing the accuracy of this approach is to choose two very dissimilar subspaces for approximation

* Approximation in an N-dimensional subspace leads to a set of N linear equations to be solved by well-known matrix inversion methods.

and then compare the attained results. One subspace choice was that spanned by a set of N equally-spaced pulses[3] (that is, we sample the field at N points along the x or y axis). In this case, R is determined by averaging the coefficients of the pulses. Other bases used were the first N modes, $e_{y_n}(y)$ and $\psi_m(x)$. In the case of e_{y_n}, R is determined directly from only the coefficient of the $e_{y_0}(y)$ term.

We made a number of additional checks on the solutions. We observed the convergence of the solutions with increasing N, and we verified the conservation of energy between incident, transmitted, and reflected waves. For certain angles of incidence we compared the results with those obtained previously by Marcuvitz and Lewin.[12,13] We also checked some of the results against values for R obtained experimentally. (See Ref. 5 for example.) We checked the thin dielectric sheath results (using the exact formula (10) for example) against thick dielectric sheath results (using the approximate formula (8) and subsequent application of the transmission line equations to the dominant mode).

In the thick sheath numerical results which follow, we restrict the results to include only the cases wherein at most a single propagating mode exists in any region where relative ϵ is greater than one.

III. DIELECTRIC LOADING RESULTS

We first consider the dielectric-loaded array (top of Fig. 2). In reality this may be viewed as an infinitely thick sheath with only one dielectric boundary interacting with the array interface ($z = 0$). The phase of R, the reflection coefficient, and the amplitude of R are plotted as a function of scan angle ($kb \sin \theta$ for the H-plane, and $kd \sin \theta$ for the quasi-E plane), with ϵ as a parameter. A moderate, but fixed, guide wall thickness in the plane of scan is assumed in all the data.

3.1 *H-Plane Results*

Fig. 3 gives some typical results for the H-plane scan direction with the waveguides loaded with $\epsilon = 0.9$ to $\epsilon = 3.0$. The change in R with ϵ between curves is smooth. Between $\epsilon = 0.9$ and $\epsilon = 1.1$, however, the change in $| R |$ is great. This may be attributed to the fact that cutoff of the dominant waveguide mode occurs at $\epsilon = 0.872$.

We notice that for $\epsilon \sim 1.3$, the angular response is nearly flat, both in amplitude and phase. In fact, for all wavelengths examined there appears to be at least one value of ϵ for which a nearly flat angular response for R is obtained. It should be noted that even if the magni-

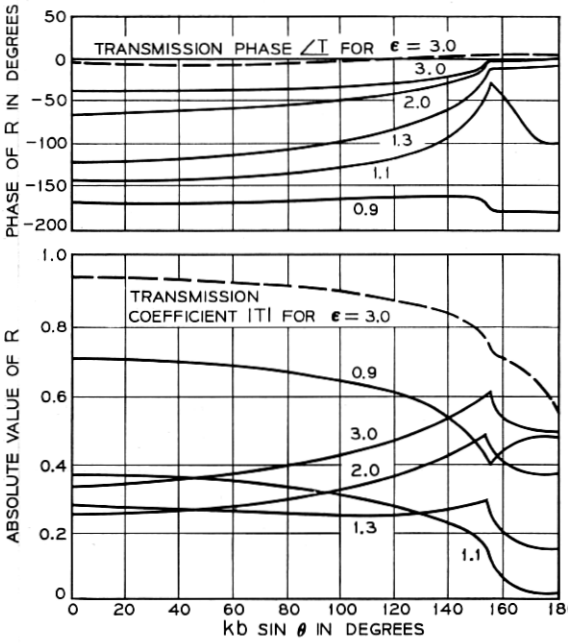

C_n = COUPLING TO nTH REMOVED ELEMENT

ϵ	$\lvert C_0 \rvert$	$\lvert C_1 \rvert$
0.9	0.626	0.015
1.1	0.252	0.080
1.3	0.202	0.094
2.0	0.319	0.106
3.0	0.423	0.081

Fig. 3 — Dielectric loading inside waveguides for H-plane scanning. $a = 0.937b = 0.5354\lambda$, $b = 0.5714\lambda$.

tude of R were large, the flatness of the response in both amplitude and phase permits matching the array for all angles in the region of flat response, at least at one frequency.

The discontinuity in slope of these curves at $kb \sin\theta = 2\pi(1-\lambda/b)$ coincides with the onset of a grating lobe at that angle. Notice that the singularity in the derivative of the modulus of R ($\lvert R \rvert$) lies on the right side of grating lobe incipience, but on the left side for the phase of R. This is the same as that found for thin walls[1, 2] and it is plausible that this will lead to the same asymptotic coupling.

The table in Fig. 3 shows the self-reflection coefficient C_0 and the coupling to the adjacent element C_1 when a single waveguide element is excited and the others merely terminated with a perfect match. The adjacent element coupling is found to be an order of magnitude smaller for the H-plane than for the quasi-E plane. For $\epsilon = 3.0$, some higher-order coupling coefficients for the H-plane case of Fig. 3 are:

$\lvert C_0 \rvert$	$\lvert C_1 \rvert$	$\lvert C_2 \rvert$	$\lvert C_3 \rvert$	$\lvert C_4 \rvert$
0.423	0.081	0.032	0.017	0.013

Fig. 3 also shows the transmission phase and amplitude curves for $\epsilon = 3.0$. These curves are in fact the far field patterns when a single waveguide element is excited[4] (except that the maximum value for θ is somewhat less than 90° since $b/\lambda > \frac{1}{2}$). The very flat phase curve is an indication that the phase center for the singly excited element lies in the aperture plane.

For a wavelength further removed from the waveguide cutoff length, the variation of R between curves of constant ϵ is considerably reduced. Fig. 4 gives some typical results for $b/\lambda = 0.400$. (The dielectric loading here permits an element spacing of less than $\lambda/2$.)

3.2 *Quasi-E Plane Results*

Fig. 5 gives typical quasi-E plane results, where $R(\theta)$, $| C_0 |$, and $| C_1 |$ are shown as a function of ϵ from $\epsilon = 0.8$ to $\epsilon = 1.6$. This range of ϵ generally depicted all the important characteristics observed. Furthermore, a slightly greater value of ϵ than $\epsilon = 1.6$ would cause the waveguides to multimode (more than one mode propagates). Notice

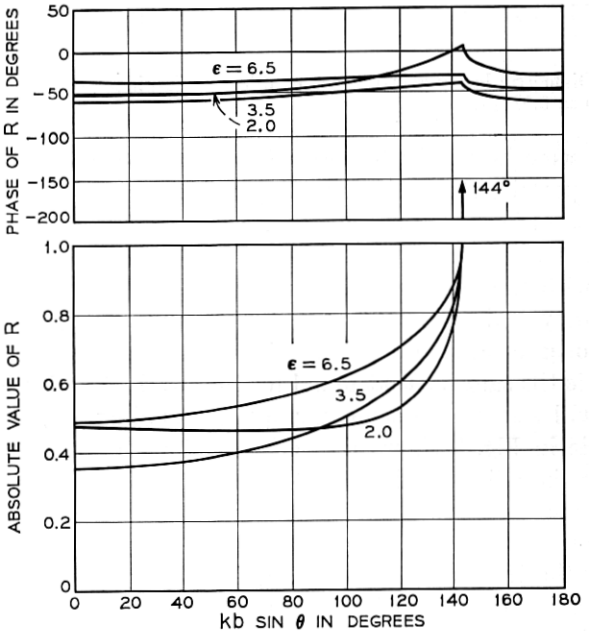

Fig. 4 — Dielectric loading inside waveguides for H-plane scanning (element spacing $< \lambda/2$). $a = 0.937b = 0.3748\lambda$, $b = 0.400\lambda$.

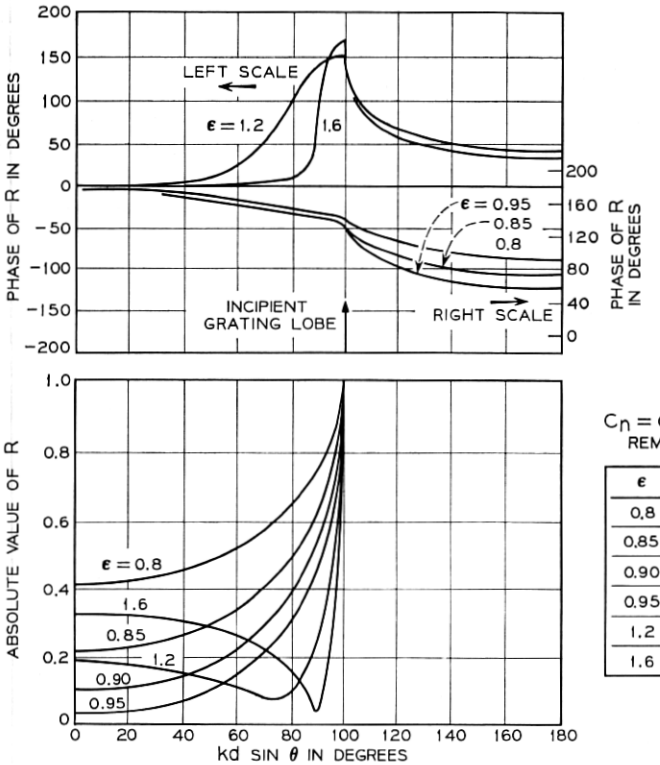

C_n = COUPLING TO nTH REMOVED ELEMENT

ϵ	$\lvert C_0 \rvert$	$\lvert C_1 \rvert$
0.8	0.661	0.308
0.85	0.548	0.331
0.90	0.502	0.330
0.95	0.480	0.324
1.2	0.473	0.294
1.6	0.515	0.245

Fig. 5 — Dielectric loading inside waveguides, for quasi-E plane scanning. $a = b = d = 0.5714\lambda$, $h = c = 0.937d = 0.5354\lambda$.

in the table of coupling coefficients that the adjacent element coupling magnitudes are an order of magnitude greater than those for the H-plane scan case, independent of dielectric constant. This is also true for higher coupling coefficients for the case depicted in Fig. 5, as shown below:

$\lvert C_0 \rvert$	$\lvert C_1 \rvert$	$\lvert C_2 \rvert$	$\lvert C_3 \rvert$	$\lvert C_4 \rvert$
0.515	0.245	0.153	0.102	0.075

This behavior is attributable to both element spacing and polarization. (By making $b < \lambda/2$, and with an appropriate dielectric loading, H-plane results very similar to these quasi-E plane results are obtainable. For example; see Fig. 4. The λ we refer to here is that which is appropriate at the aperture for $z > 0$.)

The curves of $|R|$ in Fig. 5 show that total reflection occurs beyond a critical angle ($\sim$100°). This occurs because the element spacing d is less than $\lambda/[4 - (\lambda/b)^2]^{\frac{1}{2}}$. Again, the infinite slopes for $|R|$ and for the phase of R, which occur at this critical angle, exhibit the same behavior found in the thin wall analysis[1,2] when $\epsilon = 1$. Hence the same asymptotic behavior of coupling, exp $(-jkr)/r^{\frac{3}{2}}$, may be expected for thick walled dielectric loaded arrays. (Here r is the distance between the excited and coupled element.)

A point of special interest in connection with these curves is the appearance of a resonance that occurs near the critical angle. A sharp dip in $|R|$ occurs precisely at the same angle for which the slope of the phase of R curves has a maximum. Although the sharpness of the resonance increases gradually with ϵ, it is interesting that there is no resonance for $\epsilon < 1.0$.

Fig. 6 illustrates the transmission phase and amplitude, or equivalently, the far field pattern of a singly excited element.

In Fig. 7 we illustrate the effect of a capacitive iris loading (that results when $h < c$) together with dielectric loading. In this case we

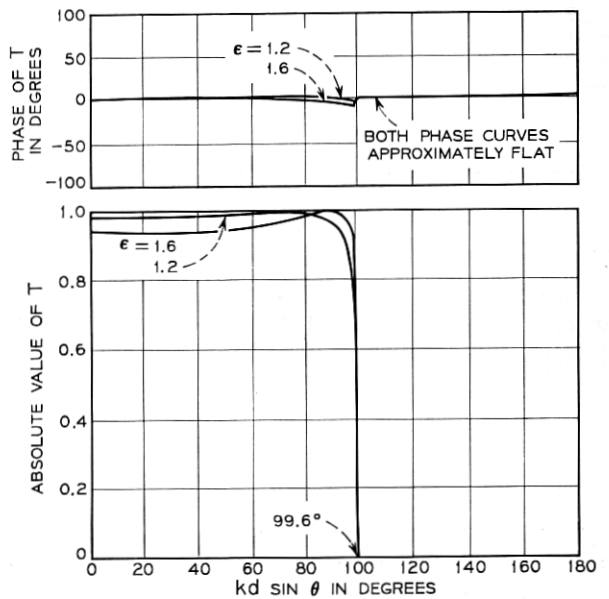

Fig. 6 — Transmission coefficient for dielectric loading inside waveguides, with quasi-E plane scanning. $a = b = d = 0.5714\lambda$, $h = c = 0.937d = 0.5354\lambda$.

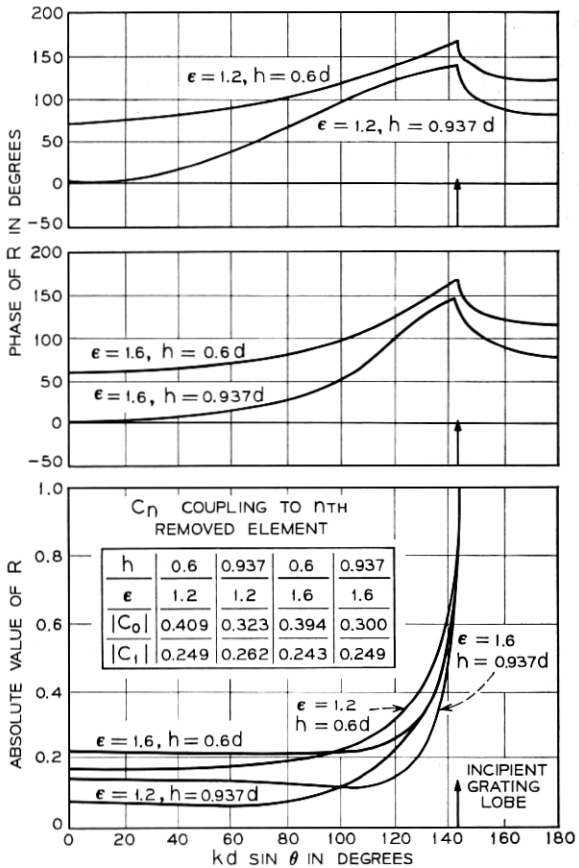

Fig. 7 — Dielectric loaded waveguides and iris loaded apertures, for E-plane scanning. $a = b = \infty$, $d = 0.400\lambda$, $h = 0.6d = 0.240\lambda$ and $h = 0.937d = 0.3748\lambda$, $c = 0.937d$ ($h = 0.937d \Longrightarrow$ fully open aperture; $h < 0.937d \Longrightarrow$ iris at aperture).

have let $a = b \rightarrow \infty$ so that a true E-plane scan in a parallel plate array is considered. The effect of the iris tends to flatten the phase and amplitude responses, particularly the phase response, at the expense of a somewhat greater average $| R |$. The larger average $| R |$ can, however, be uniformly reduced for all scan angles in a region of flat $R(\theta)$ response.

The solutions of the integral equations (1) and (2) are actually complete solutions of the boundary value problem. The fields as well as the scattering matrix are determined. The variation of E_y in the

aperture as a function of scan angle ($kd \sin \theta$) is sharper when the waveguides are loaded. Particularly interesting is the field change near the critical angle $kd \sin \theta = \lambda/[4 - (\lambda/b)^2]^{\frac{1}{2}}$, which has the value 99.57° for the results shown in Fig. 8. Since the relevant eigenvalue equation (See p. 157 of Ref. 4.) for $[E_y(\theta) + E_y(-\theta)]$ has a Hermitian kernel* for $| kd \sin \theta | > 99.57°$, the phase of $[E_y(\theta) + E_y(-\theta)]$ should be constant in this region. By observing the phase of the approximate field

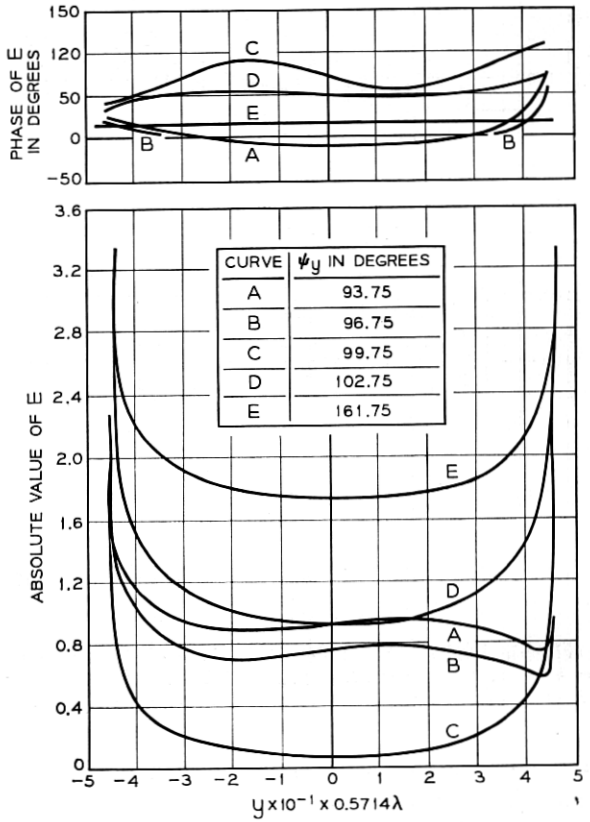

Fig. 8 — Tangential electric field distribution, $E_y(y)$, in the aperture plane, for quasi-E plane scanning. $\epsilon = 1.6$, $a = b = d = 0.5714\lambda$, $c = h = 0.937d = 0.5354\lambda$, ψ_y cutoff = 99.57°.

* Since no power is radiated for $| kd \sin \theta | > \lambda / [4 - (\lambda/b)^2]^{\frac{1}{2}}$ when the phasing is directed in the $+\theta$ and $-\theta$ directions simultaneously, the phased array behaves like a closed system, a cavity, and it is easy to show that a Hermitian kernel results. It is well known, then, that the eigenfunctions (the field solution here) of such a kernel have no varying phase.

solution at angles greater than the critical angle, we may obtain some evaluation of the errors in this solution. For most angles the errors are small. However, it is evident that errors in phase do occur for θ near the critical angle and also for y near the singularity obtained for $|E_y|$. Nevertheless, since the computation of R is an averaged quantity over the range of y, these errors do not greatly affect the values obtained for R.

IV. DIELECTRIC SHEATH INSIDE WAVEGUIDES

When we add another dielectric boundary inside the waveguides, that is, when we place a dielectric sheath inside the guides, the results obtained for R are substantially different. This is true despite the fact that we will consider only thick sheaths, in the sense described earlier. The large change in $R(\theta)$ behavior occurs because, even when a thick sheath is assumed, the second dielectric boundary is accounted for by a bilinear transmission line transformation which changes the input variation of R with θ. (A linear transformation would leave $R(\theta)$ functionally unchanged.)

In the following we will keep the dielectric constant fixed and plot $R(\theta)$ versus $kb \sin \theta$ with d_s, the sheath thickness, as a parameter. The phase of R will be referred to the aperture plane, $z = 0$, although R is the reflection coefficient for, or into, the region $z < -d_s$. The choice of ϵ in any given figure was made so that the illustrated results were typical of a wider range of ϵ. With the thick sheath approximation, the results will repeat every half guide wavelength, so that d_s is varied over only one half wavelength. The minimum d_s for which the thick approximation is valid is determined by the relative decay of the first evanescent mode in the distance d_s. This decay factor, df, is presented with each curve. It is found, generally, that $df \lesssim 0.1$ is sufficient for the thick sheath approximation to be valid. This result is usually satisfied for some $d_s \gtrsim \lambda_0/2$. Of course, by adding a sufficient number of multiples of a half guide wavelength to d_s, the results must become valid to any accuracy desired.

4.1 *H-Plane Scan Results*

In Fig. 9 we have illustrated some typical results with $\epsilon = 2.0$. For any given ϵ we have found that there exists a thickness, d_s, for which both the amplitude and phase of the reflection coefficient is flat over the generally useful region of scan angle (region in which only one lobe radiates). However, as the dielectric constant is increased, the

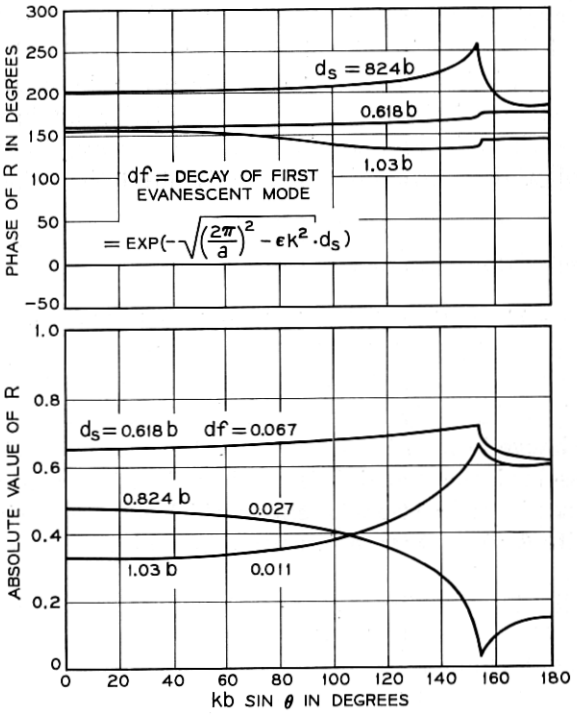

Fig 9 — Dielectric sheath inside waveguides, for H-plane scanning. $\epsilon = 2.0$, $\epsilon_1 = 1.0$, $a = 0.937b = 0.5354\lambda$, $b = 0.5714\lambda$.

frequency sensitivity of the angular response is increased. This is manifested, basically, by an increased spread between the curves shown. Furthermore, since the nearly flat curve also is found to have the maximum amplitude of R ($d_s = 0.618b$ in Fig. 9), the necessity of matching out a larger $| R |$, when ϵ is greater, further aggravates the frequency sensitivity problem that occurs with increasing ϵ. The results in Fig. 10, when compared with those in Fig. 9, show the effect of increasing ϵ.

4.2 *Quasi-E Plane Scan Results*

Qualitatively similar results are obtained in the quasi-E plane scan case as illustrated in Figs. 11 and 12. The increasing dielectric constant, illustrated by comparing the results in Figs. 11 and 12 ($\epsilon = 1.2$ and $\epsilon = 1.6$, respectively), causes a greater spread between curves and, consequently, a greater frequency sensitivity.

In addition, we again notice a sharp resonance here (increasingly sharper with greater ϵ), just as we noticed when only a single dielectric boundary was present. The primary difference between these results and those for a single dielectric boundary is that we may keep the dielectric constant fixed here and vary the thickness, d_s, to obtain a flat response. This is done, however, with the cost of increased frequency sensitivity.

V. DIELECTRIC SHEATH OUTSIDE WAVEGUIDES

We notice that very similar results are obtained in the quasi-E plane scan independent of whether the second dielectric boundary is placed inside or outside the waveguides; that is, independent of whether there is a dielectric sheath inside or outside the waveguides. Fig. 13 illustrates a typical result. In this figure the value of ϵ is held fixed while the sheath thickness (see the bottom figure of Fig. 2) is varied from curve to curve.

Notice first that when the interaction between the second dielectric

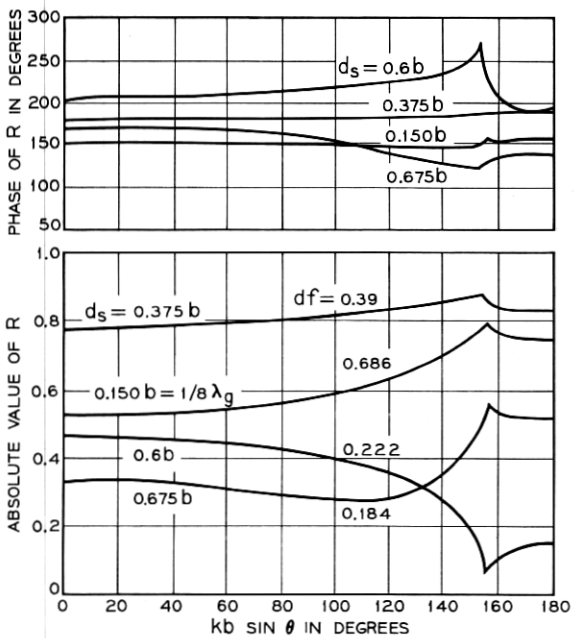

Fig. 10 — Dielectric sheath inside waveguides, for H-plane scanning. $\epsilon = 3.0$, $\epsilon_1 = 1.0$, $a = 0.937b = 0.5354\lambda$, $b = 0.5714\lambda$.

boundary, at $z = +d_s$, and the array face is accounted for, with all the evanescent modes, then the results shown by the circles and triangles are obtained. The results agree very well with those results in which higher order mode interaction with the second dielectric boundary is neglected, that is, the sheath satisfies the earlier specified thickness criteria.

Fig. 14 shows a useful way of estimating what value of d_s will be properly "thick". Notice first that the rate of decay of higher order modes away from the array face is a function of scan angle in the exterior sheath case. Hence, a single value cannot be used as a decay factor for all θ. In Fig. 14, however, the actual ratios of the first and second evanescent mode amplitudes to the propagating modes is

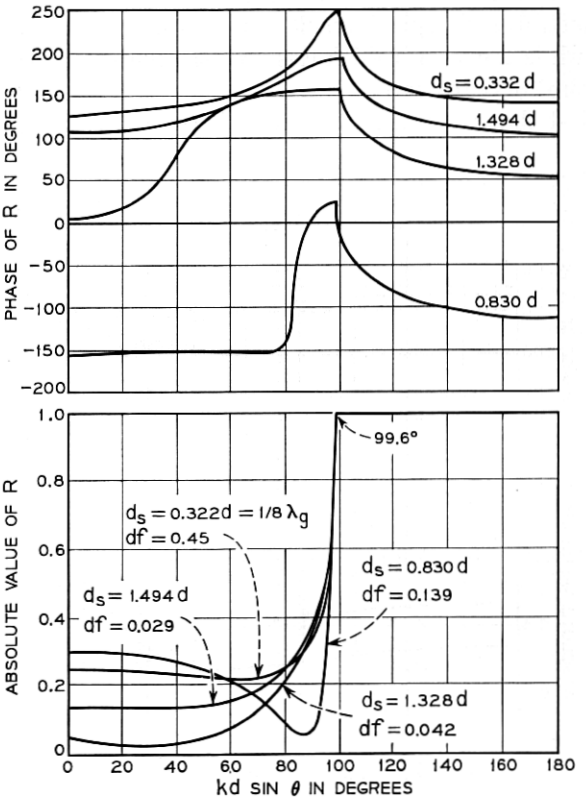

Fig. 11 — Dielectric sheath inside waveguides, for quasi-E plane scanning. $\epsilon = 1.2$, $\epsilon_1 = 1.0$, $a = b = d = 0.5714\lambda$, $c = h = 0.937d = 0.5354\lambda$.

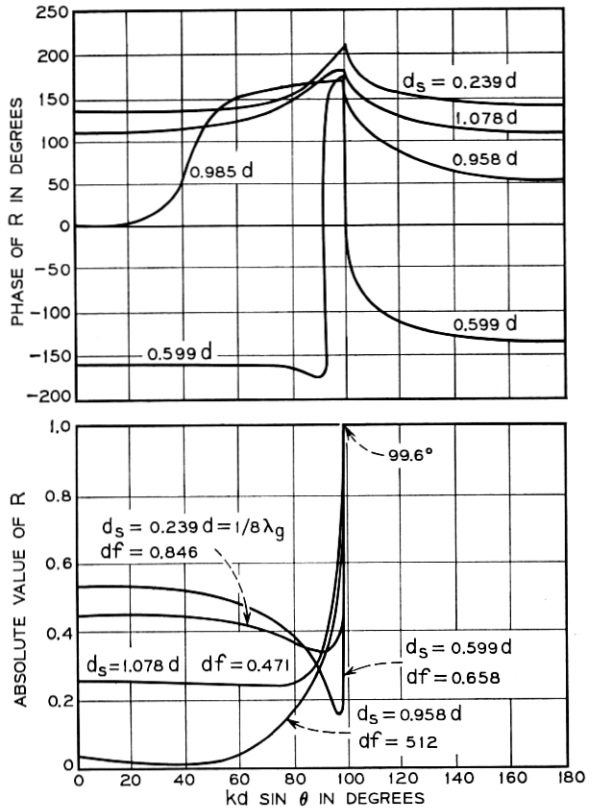

Fig. 12 — Dielectric sheath inside waveguides, for quasi-E plane scanning. $\epsilon = 1.6$, $\epsilon_1 = 1.0$, $a = b = d = 0.5714\lambda$, $c = h = 0.937d = 0.5354\lambda$.

plotted versus kd sin θ. Again we see that if $RD1$ and $RD2$ (see Fig. 14 for definitions) are less than about 0.1, then the particular d_s is thick.

A "thick" d_s means that, for a *given scan angle,* the results for $R(\theta)$ will repeat periodically so that

$$R\left(\theta, ds + n\frac{\lambda_{z\epsilon}}{2}\right) = R(\theta, d_s)$$

for all $n > 0$. The question remains whether $\lambda_{z\epsilon} = 2\pi/\beta_0'^{\epsilon}$ (see equation (7)) varies rapidly with kd sin θ. This may be answered by examining the grating lobe structures in the dielectric sheath as compared with that in free space, as shown in the inset in Fig. 13. This structure is obtained

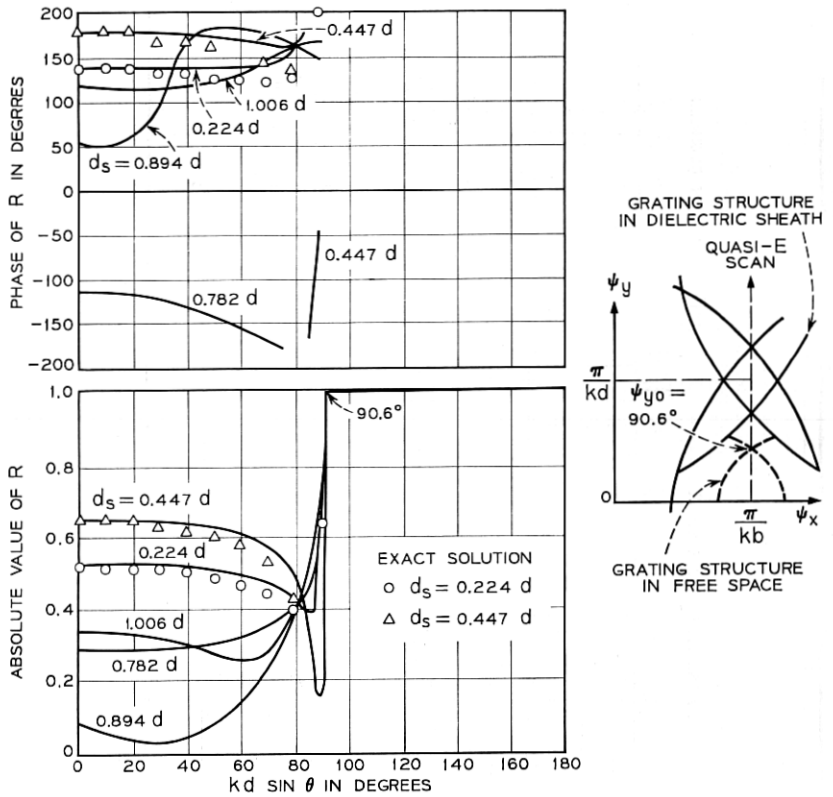

Fig. 13 — Dielectric sheath outside waveguides, for quasi-E plane scanning. $\epsilon = 1.818$, $a = b = d = 0.5596\lambda$, $c = h = 0.937d = 0.5243\lambda$.

by setting

$$\text{and} \begin{cases} \beta'^{e}_{m_\epsilon} = 0 = \sqrt{\epsilon k^2 - \left(\frac{\pi}{b}\right)^2 - \left(\frac{2\pi m - \psi_v}{d}\right)^2} & (\psi_v \equiv kd \sin\theta) \\ \beta'^{e}_{m_0} = 0 = \sqrt{k^2 - \left(\frac{\pi}{b}\right)^2 - \left(\frac{2\pi m - \psi_v}{d}\right)^2}. \end{cases} \tag{12}$$

(Actually (12) defines the intersections shown in the Fig. 13 inset. The total grating lobe structure requires setting the two-dimensional z-directed propagation constants to zero.) Now the z-directed wavelength in the sheath is given by

$$\lambda_{z\epsilon} = \frac{2\pi}{\beta'^{e}_{0_\epsilon}},$$

which is a slowly-varying function of θ in that part of the grating lobe structure bounded by the dashed lines in the Fig. 13 inset. Only this region is useful, because the propagating wave in the dielectric is totally reflected at $(kd \sin \theta)^2 \geqq k^2 - (\pi/b)^2 (\psi_v \geqq 90.6°)$. Hence the pole in λ_{ze} doesn't affect the variation of λ_{ze}, and λ_{ze} varies very little with θ, from $\psi_v = 0$ to $\psi_v^2 = (k^2 - (\pi/b)^2)$, providing that

$$\frac{\sqrt{\epsilon - 1}}{\sqrt{\epsilon - \left(\frac{\lambda_0}{2b}\right)^2}} \sim 1. \tag{13}$$

We should mention that the quasi-E plane results for the sheath inside and outside the waveguides are similar, primarily because of the element spacing that causes total reflection to occur at the defined critical angle. When the element spacing is changed, very markedly different results can be obtained. The results depicted in Fig. 15 for the H-plane are typical of this.

In examining the grating lobe diagram in the inset of Fig. 15 we notice that, in the shaded region, *two waves* propagate in the dielectric sheath whereas only *one wave* propagates in free space. This is a potentially very useful operating region for the phased array because

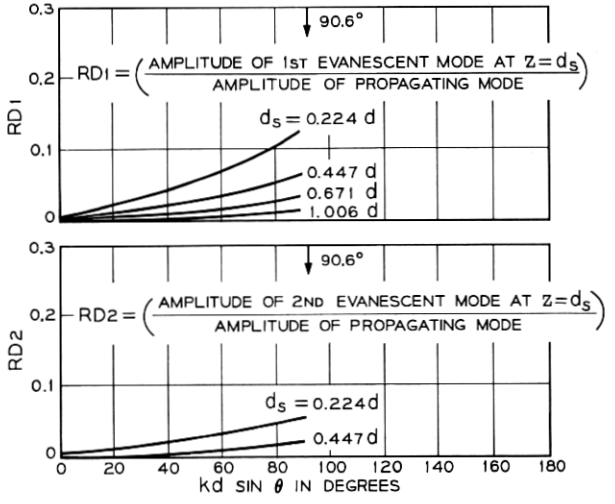

Fig. 14 — Validity check of transmission line approximations, for quasi-E plane scanning with a dielectric sheath outside waveguides. $\epsilon = 1.818$, $a = b = d = 0.5596\lambda$, $c = h = 0.937d = 0.5243\lambda$.

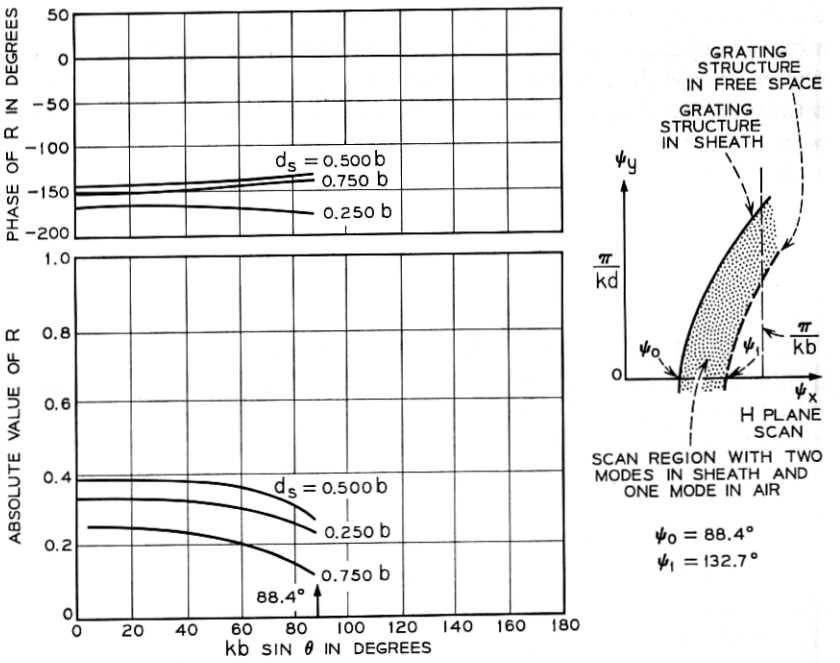

Fig. 15 — Dielectric sheath outside waveguides, for H-plane scanning. $\epsilon = 1.429$, $a = 0.937b = 0.5915\lambda$, $b = 0.6313\lambda$.

only one beam will be radiated. However, we find that interference between the two propagating waves in the dielectric causes some very interesting anomolous results associated with what might be described as unattenuated surface waves. This effect is markedly different from that which may occur for a sheath inside the guides (although as a function of frequency or sheath thickness, as opposed to scan angle, similar results may occur). Further discussion on this subject is deferred to another paper.[11]

The results in Fig. 15 for the $|R|$ and the phase of R are shown in the scan angle region in which only one wave, at most, propagates in the sheath. In this angular region the results are also very different than those for the interior sheath in that the response is comparatively flat for a wide range of sheath thicknesses.

VI. CONCLUSIONS

In summary we may state that dielectric loading or covering has a very substantial effect on the array performance to the extent that an

array and dielectric cover should be designed as an integral unit instead of being designed for minimal effect or match correction. Nevertheless, the additional parameters available in the design of an array with a dielectric cover can be used to match the array over a wide angular and frequency region.

No particular method of loading or covering appears to be universally superior except that when only one dielectric boundary is present (Fig. 2, top), the wide angle match appears to be less frequency sensitive than when a sheath or two boundaries are present. Furthermore, with thick sheaths, the maximum permissible value of ϵ is small before serious matching problems occur (a large $|R|$ together with a flat $R[\theta]$). Finally, by placing the sheath inside the waveguides instead of outside, certain anomolous reflection phenomena, associated with the exterior sheath grating lobe structure and surface waves, can be avoided.[11]

Although we did not give analytic proof, the numerical results do indicate that the asymptotic behavior of the coupling coefficients[2] is not altered by the presence of the dielectric materials.

REFERENCES

1. Wu, C. P. and Galindo, V., Properties of a Phased Array of Rectangular Waveguides with Thin Walls, *IEEE Trans.* on Antennas and Propagation, *AP-14,* No. 2, 1966, pp. 163–172.
2. Galindo, V. and Wu, C. P., Asymptotic Behavior of the Coupling Coefficients for an Infinite Array of Thin-Walled Rectangular Waveguides, IEEE Trans. on Antennas and Propagation, *AP-14,* No. 2, March 1966, pp. 248–9.
3. Galindo, V. and Wu, C. P., On the Asymptotic Decay of Coupling for Infinite Phased Arrays, paper presented at International Union of Radio Science, Washington, D. C., April 1966. (To be published.)
4. Galindo, V. and Wu, C. P., The Relation Between the Far-Zone Pattern of the Singly Excited Element and the Transmission Coefficient of the Principal Lobe in an Infinite Array, IEEE Trans. on Antennas and Propagation, *AP-14,* No. 3, March 1966, pp. 397–398.
5. Galindo, V. and Wu, C. P., Numerical Solutions for an Infinite Phased Array of Rectangular Waveguides with Thick Walls, IEEE Trans. on Antennas and Propagation, *AP-14,* 1966, pp. 149–158.
6. Galindo, V. and Wu, C. P., Integral Equations and Variational Expressions for Arbitrary Scanning of Regular Infinite Arrays, IEEE Trans. on Antennas and Propagation, *AP-14,* No. 3, May 1966, pp. 392–394.
7. Galindo, V. and Wu, C. P., A Variation Expression for the Dominant Mode Coupling Coefficients Between The Elements in an Infinite Array, IEEE Trans. on Antennas and Propagation, *AP-14,* No. 5, September 1966, pp. 637–639.
8. Magill, E. G. and Wheeler, H. A., Wide Angle Impedance Matching of a Planar Array Antenna by a Dielectric Sheet, IEEE Trans. on Antennas and Propagation, *AP-14,* 1966, pp. 49–53.
9. Lee, S. W., Impedance Matching of an Infinite Phased Array by Dielectric Sheets, IEEE Elec. Letters, *2,* No. 10, October 1966, pp. 366–368.

10. Kantorovich, L. V. and Krylov, V. I., *Approximate Methods of Higher Analysis,* Interscience Publishers, New York, 1958.
11. Wu, C. P. and Galindo, V., Surface-Wave Effects on Dielectric Sheathed Phased Arrays of Rectangular Wave-Guides, B.S.T.J. *47,* No. 1, January 1968, pp. 117–142 (next article in this issue).
12. *Waveguide Handbook,* N. Marcuvitz, ed., MIT Radiation Lab. Series, *10,* McGraw-Hill Book Company, Inc., New York, 1951.
13. Lewin, L., *Advanced Theory of Waveguides,* Iliffe and Sons, Ltd., London, 1951.